Modified diffusion-limited aggregation simulation of electrodeposition in two dimensions

Susan C. Hill and J. Iwan D. Alexander
Center for Microgravity and Materials Research, University of Alabama in Huntsville, Huntsville, Alabama 35899
(Received 9 December 1996; revised manuscript received 5 May 1997)

A modified diffusion-limited aggregation model that includes a uniform drift simulates the process of electrodeposition. Through a systematic variation of the model's parameters, aggregates (electrodeposits) grown under different simulation conditions (experimental conditions of the voltage, current density, and concentration) develop as open dendritic or as compact mossy forms. The resulting aggregate morphologies are characterized by geometric quantities derived from the aggregate particle position distribution. Power laws relate the geometric quantities to each other. Ohm's law is obeyed to lowest order in the aggregate surface curvature where the curvature is an effective conductivity. The distribution of open sites and its moments, which are geometric quantities, are introduced. [S1063-651X(97)15908-6]

PACS number(s): 81.10.Aj, 82.45.+z, 81.05.Bx

I. INTRODUCTION

The growth of metal aggregates by electrodeposition [1–4] is simulated using a modified diffusion-limited aggregation (DLA) [5,6] model. The DLA model is well suited for simulating electrodeposit growth since it can be modified to include the electrodynamic transport processes important to this problem. In the original DLA model a particle pursues an unbiased random walk in the bulk and when it arrives at the surface of the growing aggregate it attaches with a probability of unity. A fractal or dendritic aggregate growth pattern results that effectively predicts certain dendritic morphologies of electrodeposits grown in thin horizontal layers [7–12]. A modified DLA model that includes a uniform drift [13–16] and an adjustable attachment probability can also simulate the growth of compact mossy aggregates. It has already been demonstrated [17–19] that modified DLA-type simulations yield useful information regarding the evolution of crystal morphologies. The model investigated here should lead to a better understanding of the processes active during electrodeposit growth and their effects on the resulting electrodeposit morphologies.

In the model, bulk (liquid) electrolyte diffusion and migration are simulated using biased random walkers which represent the species to be deposited. The bias is characterized by an adjustable drift distance δ, which represents $|\Delta\phi|$, the magnitude of the applied potential. Surface attachment (including the reduction reaction) is included in the model via the introduction of an adjustable global sticking coefficient κ, which represents $j/|\Delta\phi|$, where j is the current density. The electrolyte bulk concentration c is controlled by an adjustable source line offset σ [20].

Through a systematic variation of the simulation parameters δ and κ at a fixed value of σ (thermodynamic conditions of $\Delta\phi$ and j at fixed c), the simulated electrodeposits develop as open dendritic or as compact forms. The transition from compact to dendritic morphologies is seen to arise as a combined result of the bulk (electrolyte) diffusion and migration and the bulk (electrolyte) aggregate (electrodeposit) interfacial kinetics. The characterization of the morphologies of the aggregates is the emphasis of this study. This is done using geometric quantities of the aggregates that are derived from the aggregate particle position distribution. These include fractal dimension, density, aggregate surface mass exponent, average aggregate surface curvature, and the probability density of open sites, or neighborhood pattern distribution, and its moments, which will be introduced here. Both qualitative and quantitative information about electrodeposit growth morphologies is obtained.

The modified DLA simulation procedure in two dimensions (2D) will be described in detail in Sec. II, and the conditions under which the simulations were made will be given. In Sec. III the process of electrodeposition and the simulation model will be connected. In Sec. IV the open site distribution will be defined and asymptotic simulation results will be given. These include plots of aggregate growth along with results for the open site distribution and other geometric quantities. A detailed discussion of the observed types of aggregate morphologies follows in Sec. V. Section VI is the conclusion.

II. MODIFIED DLA SIMULATION

The geometry of the modified DLA simulation is shown in Fig. 1. The initial state of the simulations is a horizontal seed line of particles. A source line for new walkers is initially offset σ lattice spacings from the seed line. It is then displaced so as to remain at least σ above the growing aggregate. A fixed source line offset $\sigma=15$ was used throughout these simulations and was found to adequately model aggregate growth from a dilute electrolyte at all drift distances δ lattice spacings considered here [20].

A walking particle initiated at a random point on the source line pursues a biased random walk in the bulk. The walker jumps to an open site and then drifts a fixed δ downward toward the seed line or the aggregate surface, again landing at an open site. Jumps from a site adjacent to the surface have the same *a priori* isotropic jump probability as jumps in the bulk. When $\delta>1$ the drift downward is completed gradually so that if the walker becomes adjacent to the aggregate surface the drift ceases.

On its arrival at an open or unoccupied site adjacent to an occupied site in the seed line or the aggregate surface, the walker attempts to attach. The probability that the walker

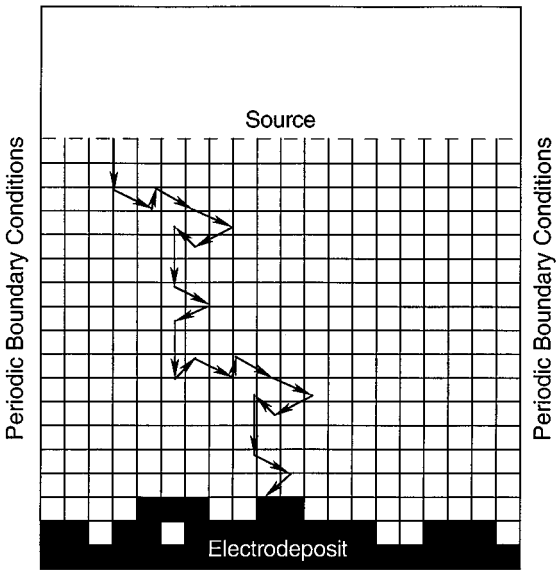

FIG. 1. Modified DLA simulation geometry in 2D illustrating a typical path of a random walker that reaches the surface.

joins the aggregate is determined by the sticking coefficient κ. A random number w, $0 \leqslant w \leqslant 1$, is generated, and if $w \leqslant \kappa$, the walker attaches. If $\kappa < 1$, the walker may fail on its first attempt to attach. It may then diffuse on the aggregate surface and make repeated attempts to attach until it finally succeeds or else returns to the bulk. If it returns to the bulk, it may reach a discard line, at which point it is discarded. A discard line offset a fixed ten lattice spacings above the source line was adequate and consistently allowed for the loss of walkers at small $\delta < 1$. In either case of the attachment or the discarding of the walker, a new walker is started and the procedure is repeated until a preset aggregate growth height is reached.

These are small mass, small time, and small radius of gyration simulations. The lateral dimension of the aggregate growth in the direction perpendicular to the drift direction was fixed at 58 lattice spacings. Periodic boundary conditions are imposed at the side boundaries. There are two phases of aggregate growth: At low growth heights there is an initial growth phase in which transients occur that is followed by an approach to asymptotic growth. To compare the different simulated morphologies, it is important to ensure that sufficient aggregation has occurred beyond the growth transient. Growth to a height of 39 lattice spacings was adequate since beyond that aggregate morphology changes were insignificant.

The simulation parameters used for the growth of aggregates included fractional drift distances in the range $0 < \delta < 1$ and integral drift distances in the range $0 \leqslant \delta \leqslant 4$. Logarithmically spaced sticking coefficients were used in the range $0.01 \leqslant \kappa \leqslant 1$. For off lattice walks, when $\delta < 1$, fractal dimension saturates and aggregate morphology apparently no longer changes much when $\kappa \leqslant 0.05$. The saturation may represent the onset of some new morphological type or it may merely be the point of failure of the simulation. If the latter is true, at very small δ the simulation should be modified to include a locally determined sticking coefficient.

III. ELECTRODEPOSITION AND THE SIMULATION MODEL

A. Bulk transport

The modified DLA simulation model and the process of electrodeposition are connected in this section. Transport in the electrolyte bulk is related to the biased random walks in the modified DLA simulation. The drift distance δ controls the bias and represents the magnitude of the overpotential. The biased random walks satisfy the discrete Smoluchowski equation [21].

In a uniform electric field the transport of ions in the electrolyte bulk occurs by diffusion and migration with a constant drift velocity. The transport is described by a parabolic differential equation derived from the Nernst-Planck equation [24,25]

$$\frac{\partial c}{\partial t} = D_0 \nabla^2 c - \mathbf{v}_d \cdot \boldsymbol{\nabla} c. \tag{1}$$

Here the concentration c is assumed to be dilute and D_0 is the bulk diffusion coefficient. The constant drift velocity where $v_d = |\mathbf{v}_d|$ is proportional to the implied force

$$v_d = \mu_{\text{abs}} q |\mathbf{E}| = \mu_{\text{abs}} q \left| -\frac{\Delta \phi}{l} \right|, \tag{2}$$

where q is the charge on the ion, μ_{abs} is the absolute ionic mobility, and l is the cell size.

Migration and diffusion of an ion in the electrolyte bulk are modeled in the modified DLA simulations by a biased random walk. The bias is characterized by the drift distance d. The probability that a walker undergoing a biased random walk can be found at the location $\mathbf{r}_k$ after k steps is [16]

$$U(\mathbf{r}_k, k\tau) = \frac{1}{c} \sum U(\mathbf{r}_{k-1}, (k-1)\tau). \tag{3}$$

The summation in Eq. (3) extends to all occupied sites at locations $\mathbf{r}_{k-1}$ from which by a single jump and drift it is possible to arrive at the location $\mathbf{r}_k$ in one step where $\mathbf{r}_k = \mathbf{r}_{k-1} + \mathbf{a} + \mathbf{d}$. The vector $\mathbf{a}$ is an unbiased random walk with equal *a priori* jumping probability to any of the four corners of a square where $\mathbf{r}_{k-1}$ is at the center of the square. This square is oriented diagonal to the axes of the underlying square lattice which has lattice spacing a, but the center and the corners of the square do not have to coincide with lattice points. The vector $\mathbf{d}$ is the uniform drift superimposed on each step of the random walk and is due to the drift velocity imposed by a uniform external electric field in a time τ, which is the mean time between collisions and will be taken to be one Monte Carlo step. The constant c is a normalization factor.

A connection can to be made to Eq. (1) by expanding Eq. (3) in a Taylor series. Such an expansion is valid so long as $\max(a,d)$ is smaller than the radius of convergence of the series. On evaluating the limits as τ and a go to zero, the Smoluchowski equation for the case of a constant, spatially independent force results:

$$\frac{\partial U}{\partial t} = D_0 \nabla^2 U - \mathbf{v}_d \cdot \boldsymbol{\nabla} U, \tag{4}$$

where the time $t = k\tau$. The diffusion coefficient D_0 and magnitude of the drift velocity v_d are [16]

$$D_0 = \lim_{\substack{\tau \to 0 \\ a \to 0}} \frac{a^2}{2\tau}, \tag{5}$$

$$v_d = \lim_{\substack{\tau \to 0 \\ a \to 0}} \frac{d}{\tau}. \tag{6}$$

The drift distance simulation parameter δ will be proportional to v_d, which is proportional to an externally imposed uniform electric field and, hence, to the applied potential.

Whether the diffusive term or the migration term is dominant in the Smoluchowski equation depends on the relative magnitude of v_d and D_0. The Peclet number [26] is defined as

$$P_e = \frac{v_d}{D_0} a = \frac{2d}{a}. \tag{7}$$

Bulk diffusion will still be important in comparison to drift provided $d \leqslant a/2$ or $P_e \leqslant 1$. As d is increased above $a/2$, the transport becomes increasingly more and more ballistic. As long as $d < a$, the probability is nonzero for escape to a distance away from the aggregate surface limited only by the size of the system. When d approaches the lattice spacing a and P_e approaches the value 2, a bifurcation in the number of available transport directions occurs from one direction to two directions. When $d \geqslant a$, the walker can only move in a direction toward the aggregate surface and the attachment is deterministic.

B. Attachment kinetics

The surface kinetics, reduction reaction, and attachment in the electrodeposition process can be described by a well-known macroscopic electrochemical equation due to Barton and Bockris [1–3]. In this case, the sticking coefficient κ represents the ratio of the current density to the magnitude of the overpotential. An elastic boundary condition [22,23] of the Smoluchowski equation is equivalent to the Barton-Bockris equation in a certain limit.

The overpotential $\eta = \Delta\phi - \Delta\phi_e$ is the difference between the electrode potential $\Delta\phi$ and the equilibrium electrode potential $\Delta\phi_e$ for the reduction reaction

$$M^+ + e^- \rightarrow M, \tag{8}$$

where M^+ is a univalent metal ion, e^- is an electron, and M is the reduced metal atom. In the modified DLA simulations $\Delta\phi_e = 0$ because the reaction occurs at drift distance $\delta = 0$. The convention that is observed here is that $\eta < 0$ is associated with $j > 0$, where j is the cathodic current density. The Barton-Bockris equation is the sum of the overpotentials due to activation, diffusion, and the Kelvin effect and is

$$-\frac{F\eta}{Nk_BT} = \frac{j}{j_0}\left(1 + \frac{r}{D_0 F c_0 / j_0}\right) + \frac{2V_m/Nk_BT}{r}\,\gamma(\eta, r). \tag{9}$$

Here r is the electrodeposit surface radius of curvature, c_0 is the bulk concentration in the electrolyte, j_0 is the exchange current density, V_m is the molar volume of adsorbed ions at the electrodeposit surface, and the surface free energy is γ.

The reduction reaction of Eq. (8) is an activated process, and the first term in Eq. (9) is due to the activation overpotential where the dependence of j on η is given by a small argument expansion of the Butler-Volmer equation [24,27,28]. The second term in Eq. (9) is due to the diffusion (or concentration) overpotential which occurs because there is a concentration gradient at the surface of the cathode due to depletion of the reacting metal ion [24,28]. According to Nernst's law, the concentration gradient gives rise to an overpotential. The radius of curvature, r, is an effective resistivity and the diffusion and activation overpotentials combine to form an equation that is basically Ohm's law.

The third term in Eq. (9) is due to the overpotential from the Kelvin effect [29,30]. At the tips of protrusions, diffusion is spherical and a shorter diffusional path exists between the surface and outer plane of the diffusion layer and deposition is therefore faster than at the flat part of the surface or at depressions. This leads to an accentuation of the potential at small radii on the electrodeposit surface [1–3]. If a potential is imposed across the surface, the surface free energy depends on the magnitude of the applied potential [24]. The curvature of a highly curved surface may also affect the surface free energy [29–32]. Equation (9) is valid at small η (i.e., in the linear regime of the Butler-Volmer equation).

A reaction that is diffusion controlled has a rate that is limited by the arrival of ions at the electrodeposit surface. It can be assumed that under this condition the total sticking probability of the ions undergoing reduction and attachment to the electrodeposit surface is unity [33,34]. This will be the case when j is greater than or equal to the diffusion-limited current density $j_L = D_0 F c_0 / L$, where L is the diffusion layer thickness. When the $j < j_L$, a sticking coefficient can be defined as the ratio $K = j/j_L$, but if $j > j_L$, then $K = 1$.

The sticking coefficient K has a physical counterpart in the ratio $j/|\eta|$. When $\eta = 0$, then $j = 0$ and L diverges in the sense that the diffusion layer extends throughout the bulk of the electrolyte and is only limited in extent by the size of the system. As η is increased from zero, L decreases monotonically [16]. Now $K = Cj/|\eta|$, where C is a proportionality constant. The simulated sticking coefficient κ will be proportional to K.

In the modified DLA simulations, the probability $U(\mathbf{r}, t)$ at location $\mathbf{r}$ after a time t will be a solution of the Smoluchowski equation, Eq. (4), subject to given boundary conditions. The sticking coefficient K for attachment to the aggregate surface [5,6,22,23] is included in the boundary condition by imposing a mixed or elastic boundary condition at the aggregate surface. For this case, with $0 \leqslant K \leqslant 1$, the boundary condition is [23]

$$KU|_s + (1-K)\{P_e \cos\theta U|_s - a\mathbf{n} \cdot \boldsymbol{\nabla} U|_s\} = 0. \tag{10}$$

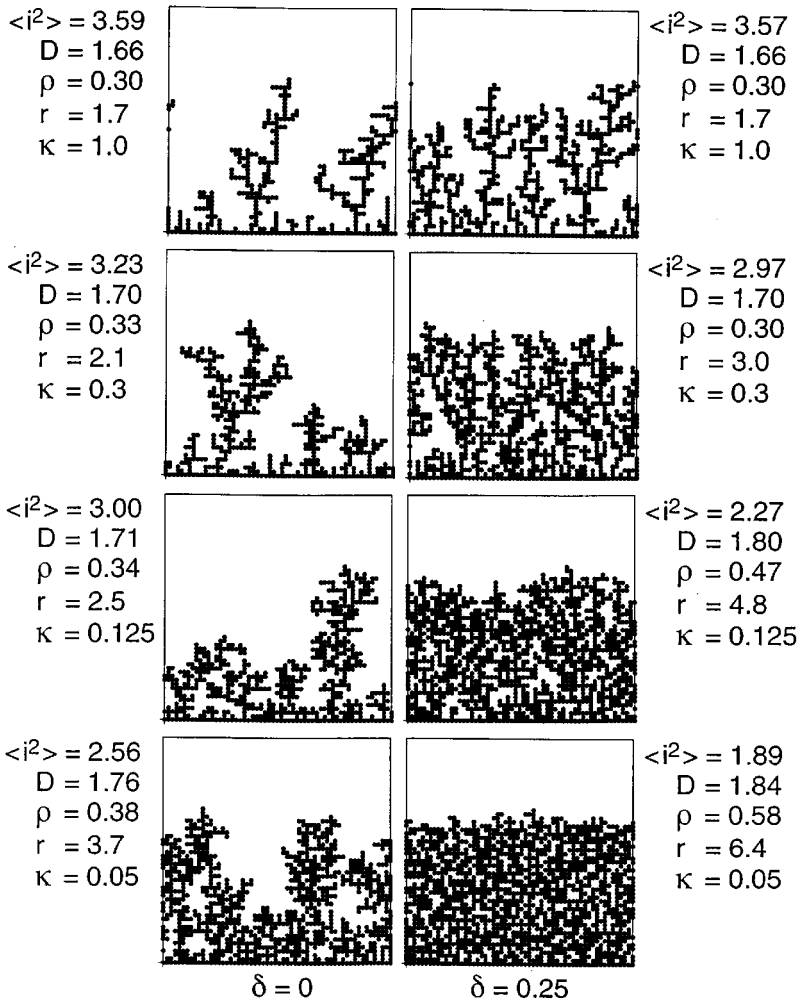

FIG. 2. Aggregate growth at a growth height $n=39$. The drift distances are $\delta=0.0$ (left) and $\delta=0.25$ (right).

Here θ is the angle between the normal to the aggregate surface and the drift direction, which are not necessarily parallel on an arbitrarily shaped boundary. In general, over the boundary layer, P_e will be nonzero.

Equation (10) can be rewritten as

$$\frac{\lambda}{a}=\frac{U|_s}{a\mathbf{n}\cdot\nabla U|_s}=\frac{1}{P_e\cos\theta+K/(1-K)}. \tag{11}$$

Here the inverse of the logarithmic derivative of the probability at the aggregate surface has introduced an adjustable length scale λ [5,6], which will be on the same scale as the radius of curvature of the aggregate surface. When the walking particle becomes adjacent to the surface of the growing aggregate in the modified DLA simulations, the drift ceases and v_d and, hence, P_e are zero. At $P_e=0$, Eq. (11) is

$$\frac{1}{K}=\frac{\lambda}{a}+1. \tag{12}$$

This expression is essentially the Ohm's law limit of Eq. (9), which includes the resistivity associated with the processes of activation and diffusion. To lowest order, the elastic boundary condition ensures that Ohm's law is obeyed on the aggregate surface.

IV. GEOMETRIC QUANTITIES OF THE AGGREGATES

A. Introduction

Aggregate growths are shown in Figs. 2–4. The sticking coefficient κ and drift distance δ vary over the plots. Details of the aggregate morphology will be discussed after asymptotic simulation results are presented for some geometric quantities.

The probability density of open sites, or neighborhood pattern distribution, and its moments are useful for characterizing the morphologies of the aggregates grown in the modified DLA simulations. The number of open or unoccupied sites that are adjacent to an occupied site at $\mathbf{r}_S$, $S=1,2,\ldots,N$, in the aggregate, $i(\mathbf{r}_S)=0,1,2,3$, is a discrete random variable which offers a well-defined statistical description of the smallest clusters of particles from which the aggregates can be built. In 2D on a square lattice $i(\mathbf{r}_S)=0$ when the occupied site at $\mathbf{r}_S$ is fully surrounded by nearest-neighbor occupied sites. The maximum value of $i(\mathbf{r}_S)=3$ because the site must be connected to the aggregate growth. Each of the four values of $i(\mathbf{r}_S)$ is associated with a particular neighborhood pattern that can develop about a given occupied site in the aggregate. The four neighborhood patterns in 2D are shown in Fig. 5.

The reduced open sites probability density $P_n(i)$, $i=0,1,2,3$, is the distribution of the four neighborhood pat-

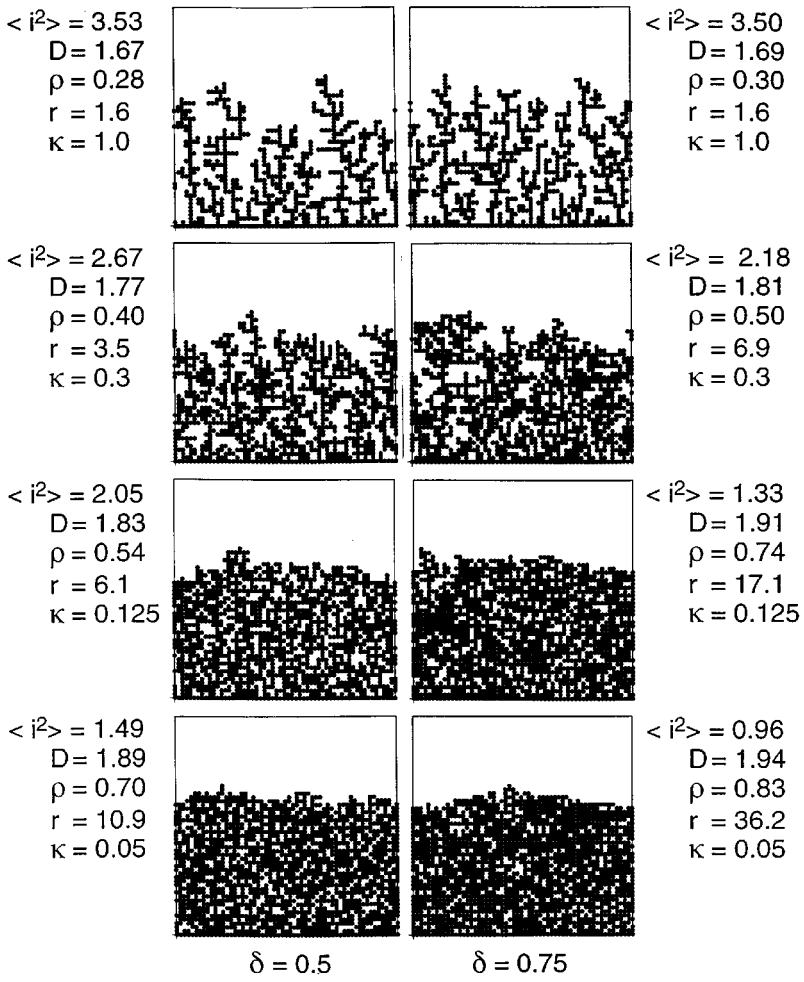

FIG. 3. Aggregate growth at a growth height $n=39$. The drift distances are $\delta=0.5$ (left) and $\delta=0.75$ (right).

terns for the entire aggregate at given time n. The expectation values of $P_n(i)$ which are most useful for examining the morphology of aggregates are the mean open sites

$$\langle i\rangle_n=\sum_{i=0}^{3} iP_n(i), \tag{13}$$

the mean square open sites

$$\langle i^2\rangle=\sum_{i=0}^{3} i^2P_n(i), \tag{14}$$

and the variance of the open sites distribution

$$\mathrm{var}(i)_n=\langle i^2\rangle_n-\langle i\rangle_n^2. \tag{15}$$

Properties of the mean square open sites $\langle i^2\rangle$ are given in the Appendix. The value $\langle i^2\rangle=1$ will be taken to distinguish between dendritic and compact morphological phases. The observed power laws relating $\langle i^2\rangle$ to other geometric quantities then determine certain morphological crossover values of those quantities. Although the choice $\langle i^2\rangle=1$ is somewhat arbitrary, the observed crossover fractal dimension and crossover density are consistent with the onset of a compact morphology.

The standard deviation of the open sites distribution is $\sigma(i)$ where $\mathrm{var}(i)=\sigma(i)^2$. In Fig. 6, $\sigma(i)$ is plotted as a function of aggregate growth height at a drift distance $\delta=1.0$ for various sticking coefficients κ. This figure shows $\sigma(i)$ for single aggregates and is a typical example of the behavior of $\sigma(i)$ with the simulation parameters. Initially, the monolayer seed line is flat so that the aggregate is made up solely of vacancy sites with $P(i=1)=1$ and $P(i)=0$, $i=0,2,3$. Initially, $\langle i\rangle$ and $\langle i^2\rangle$ are unity and $\sigma(i)$ has an initial value of zero.

Figure 6 shows the occurrence of two phases of aggregate growth. At low growth heights (less than ten lattice spacings in this example), there is an initial growth phase in which transients occur that is followed by an approach to asymptotic growth. The overshoots in the $\sigma(i)$ transients are nearly uniform in their magnitude and duration for the simulation parameters considered. These reflect the development of a characteristic rough morphology as the flat initial condition is being forgotten. The oscillations that occur after the initial growth phase damp out on averaging over several aggregates. By a growth height of 39 lattice spacings, $\sigma(i)$ has reached an asymptotic value for almost all sets of simulation parameters considered. The fractal dimension and $\langle i^2\rangle$, considered as functions of growth height, also reach asymptotic values at this stage, except perhaps at the highest κ. Simulations with much larger geometries confirm that the gross morphology of the aggregates changes little with further increases in their mass or radius of gyration. Results obtained at this growth height appear to be adequate for the analysis of the asymptotic interrelationships among and between the geometric quantities and the simulation parameters.

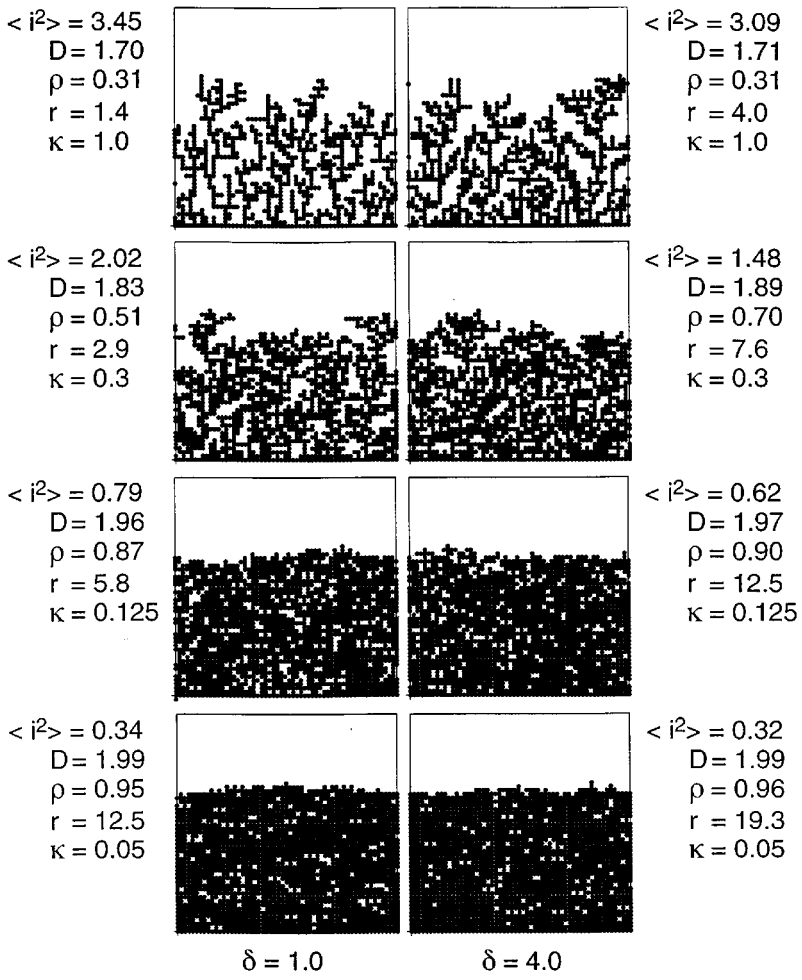

FIG. 4. Aggregate growth at a growth height $n=39$. The drift distances are $\delta=1.0$ (left) and $\delta=4.0$ (right).

B. Mean-square open sites, fractal dimension, and density

In Fig. 7, the mean-square of the open sites $\langle i^2 \rangle$ is shown as a function of sticking coefficient κ at various drift distances δ. The data for $\kappa \leqslant 0.3$ are used to estimate the crossover sticking coefficient κ^*, found when $\langle i^2 \rangle = 1$, by interpolation for $\delta \geqslant 0.75$ and by extrapolation for $\delta \leqslant 0.5$. In Fig. 8, κ^* distinguishes the morphological phases of the aggregates. As δ goes to zero, the estimated $\kappa^* > 0$, indicating that a 2D solid could be grown even in the absence of an applied electric field. For $\delta \leqslant 1$, κ^* is a nearly cubic function of δ and then for $\delta > 1$ it slowly increases. In the limit δ goes to infinity, κ^* may approach unity and Eden or ballistic clusters [35] should result.

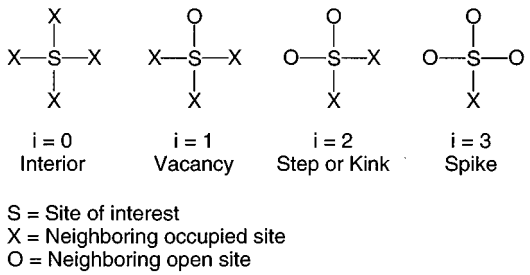

FIG. 5. Neighborhood patterns in 2D. The open sites variable is i.

The fractal dimension D is estimated statistically because of the relatively low mass and radius of gyration of the aggregates. The distribution of D is obtained for a very large sample of rectangular boxes that have a range of areas and locations, and it is sharply peaked. The average D correlates well with D obtained from plotting $\ln N(R)$ as a function of $\ln R$ where N is the mass of the aggregate. The density ρ of an aggregate is calculated from the known values of N and D.

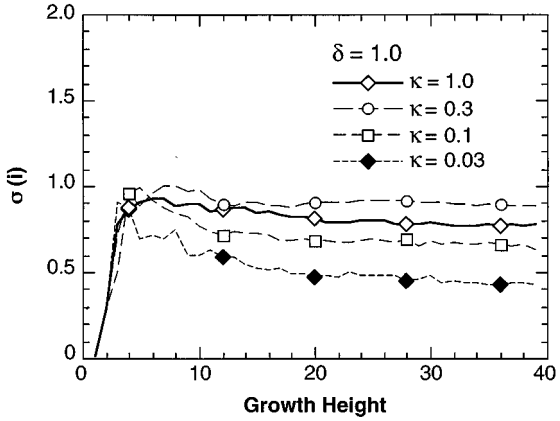

FIG. 6. Standard deviation of the open sites distribution $\sigma(i)$ as a function of aggregate growth height and various sticking coefficients κ. The drift distance $\delta=1.0$.

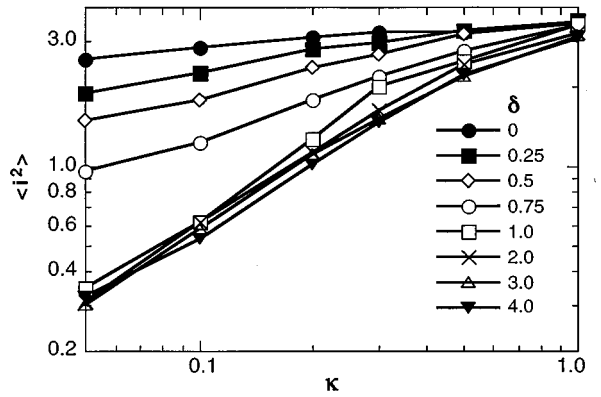

FIG. 7. Mean-square open sites $\langle i^2\rangle$ as a function of sticking coefficient κ and various values of the drift distance δ.

The mean-square of the open sites $\langle i^2\rangle$ is shown as a function of $2-D$ in Fig. 9. The aggregates represented in the plot were grown over a full range of δ and κ. The log-log plot is essentially linear except possibly at the lowest D and indicates the power law

$$\langle i^2\rangle = \left[\frac{(2-D)}{(2-D^*)}\right]^{\sigma}. \tag{16}$$

The crossover fractal dimension D^* is found when $\langle i^2\rangle = 1$. The fit parameters for the full data set are $D^* = 1.938$ and $\sigma = 0.6934$. A log-log plot of $\langle i^2\rangle$ as a function of $1-\rho$ is very similar to the plot of $\langle i^2\rangle$ versus $2-D$, indicating the power law

$$\langle i^2\rangle = \left[\frac{(1-\rho)}{(1-\rho^*)}\right]^{\zeta}. \tag{17}$$

The crossover density $\rho^* = 0.8189$ is found when $\langle i^2\rangle = 1$ and the exponent $\zeta = 0.7669$. The values of these fit parameters are roughly constant over the entire simulation parameter set.

A two-dimensional defect-free solid (i.e., no voids) of arbitrary nonfractal shape with $D = d = 2$ has $\rho = 1$, where the density has units of the number of particles per lattice spacing squared. The observed D^* and ρ^* are near these values. The DLA result $D = 1.66$ obtained with $\kappa = 1$ and $\delta = 0$ gives a minimum value of $\rho = 0.3$ in the simulation results with fairly low-mass aggregates.

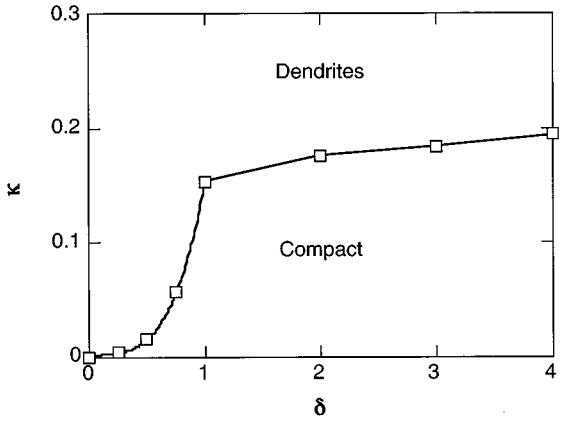

FIG. 8. The crossover sticking coefficient κ^*, shown as a function of drift distance δ, separates the dendrite and compact morphological phases.

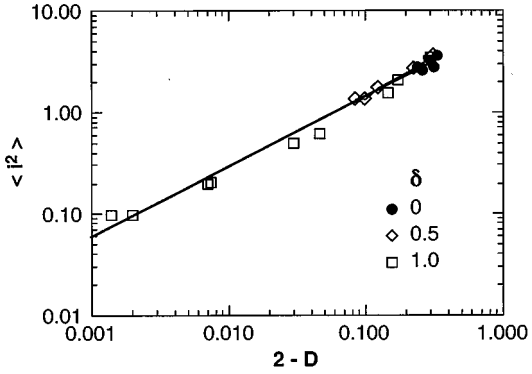

FIG. 9. Mean-square open sites $\langle i^2\rangle$ as a function of fractal dimension $2-D$ from aggregates grown over a range of sticking coefficients κ and three different values of the drift distance δ.

Plots of ρ as a function of κ at constant δ are shown in Fig. 10. Two trends in the variation of ρ are apparent in the plots. First, ρ increases systematically as δ increases, but when $\delta > 1$, ρ increases very slowly with δ. Second, as κ decreases, ρ increases. Since $\kappa = cj/|\eta|$, this means that at any constant overpotential (drift distance) the density will be highest at the lowest current densities.

C. Average aggregate surface curvature

The average curvature $1/r$ is a simple average of the local curvatures of surface sections of aggregates grown over a range of random number seeds. Lagrange interpolating polynomials [36] are fit to the surface sections and then used to estimate their local curvatures [37]. For oblate parabolic surface sections, relatively accurate local curvature estimates are obtained from three-point fits to the width and height of the surface section.

The variation of mean-square open sites $\langle i^2\rangle$ with r was examined for both 2D hemispherical solids with density $\rho = 1$ and for simulation results with varying drift distance δ and sticking coefficient κ. The following power law was found relating $\langle i^2\rangle$ to r:

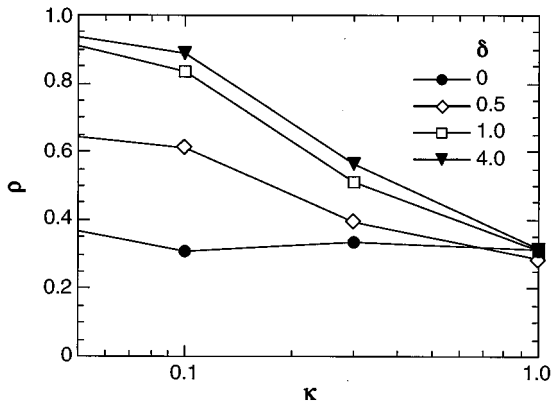

FIG. 10. Density ρ as a function of sticking coefficient κ and different drift distances δ.

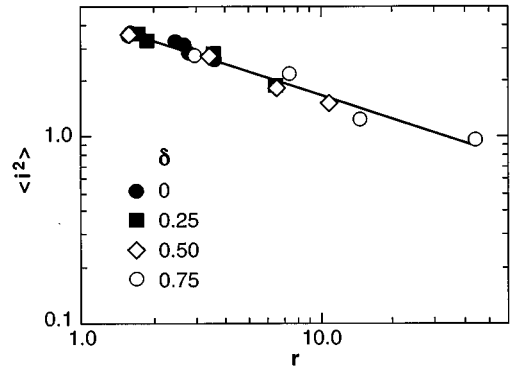

FIG. 11. Mean-square open sites $\langle i^2 \rangle$ as a function of aggregate radius of curvature r from aggregates grown over a range of sticking coefficients at drift distances $\delta < 1$.

$$\langle i^2 \rangle = \left(\frac{r^*}{r} \right)^{\chi}, \tag{18}$$

with fit parameters $r^* = 4.808$ and $\chi = 1.080$ for the 2D hemispherical solids. The crossover radius r^* is found when $\langle i^2 \rangle = 1$. A linear relationship between $\langle i^2 \rangle$ and $1/r$ is predicted in the Appendix. A model calculation that assumes a linear falloff of the density in the expression for $\langle i^2 \rangle$, Eq. (A4), gives the result $r^* = 4.828$.

Log-log plots of $\langle i^2 \rangle$ as a function of r are shown in Fig. 11 for $\delta < 1$ and Fig. 12 for $\delta \geqslant 1$ over a range of κ. The simulation results indicate the same power law as in Eq. (18). The power-law-fit parameters are for $\delta < 1$ (Fig. 11, overall data set) $r^* = 33.133$ and $\chi = 0.4236$, for $\delta = 1$ (Fig. 12) $r^* = 4.702$ and $\chi = 1.094$, and for $\delta = 4$ (Fig. 12) $r^* = 9.050$ and $\chi = 1.485$. When $\delta = 1$, the results for r^* and χ are consistent with those for 2D hemispherical solids.

In the modified DLA simulations, the average radii r of the aggregate surfaces seem to be fixed by δ and κ through some quasiequilibrium equation of state inherent in the simulations, at least in an asymptotic steady state of growth. It was demonstrated in Sec. III B that the Barton-Bockris equation is consistent with the modified DLA simulation model, at least in the large-r limit. For this reason κ was simply fit as a function of r to Ohm's law, $\kappa = A/(1+r)$, where A is a fit parameter. The Ohm's law fit for $\delta = 0.75$ shown in Fig. 13 is good. This is a low-δ fit that includes some large-r data and A is of order unity. The Ohm's law fit for $\delta = 4.0$ is very bad. Instead, the fit for $\delta = 4.0$ shown in Fig. 13 is to a modified Barton-Bockris equation that includes surface-free energy corections and is a cubic function of r. Ohm's law may be adequate for the low-δ data where there may be complete activation and diffusion control. At the larger δ, transport is ballistic, the Kelvin effect is important, and the reduction reaction is the rate limiting step.

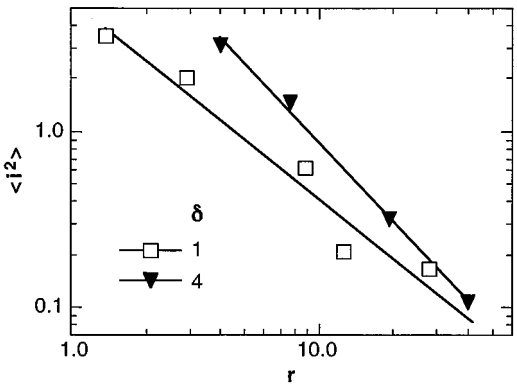

FIG. 12. Mean-square open sites $\langle i^2 \rangle$ as a function of aggregate radius of curvature r from aggregates grown over a range of sticking coefficients at drift distances $\delta = 1$ and $\delta = 4$.

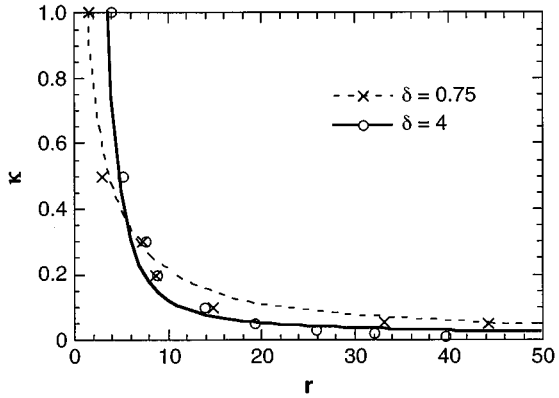

FIG. 13. Fits of the modified DLA simulation data to Ohm's law at a drift distance $\delta = 0.75$ and to a modified Barton-Bockris equation at $\delta = 4.0$. The radius of curvature is r and κ is the sticking coefficient.

D. Aggregate surface mass exponent

The aggregate surface mass exponent α [38] relates the number of particles in the aggregate surface N_S to the total mass N:

$$\alpha \approx \frac{\ln N_s}{\ln N}. \tag{19}$$

A particle is defined operationally to be part of the aggregate surface if it is a potential attachment site for another walking particle. The number of particles in the surface is either counted by hand or found using a computational search technique.

A plot of α as a function of sticking coefficient κ is shown in Fig. 14 for several drift distances δ. At large κ near unity, α approaches unity for all δ, a limit consistent with dendritic growth, which is comprised almost entirely of surface. These very high values of α at large κ are due partially to the low mass of the aggregates and the short duration time of the simulations. The exponent α decreases as δ is raised and κ is lowered, and α falls rapidly when $\kappa \leqslant 0.3$ for all δ. Values of α near 1/2 were observed in the simulations for the aggregate growths produced under the conditions of low κ and high δ.

V. DISCUSSION OF AGGREGATE MORPHOLOGY

The richness in the variety of aggregate morphology in the asymptotic growth regime is clearly displayed in the aggregates grown under various simulation conditions shown in Figs. 2–4. The morphology of an aggregate can be characterized by the geometric quantities determined by the aggregate particle position distribution. These are the most con-

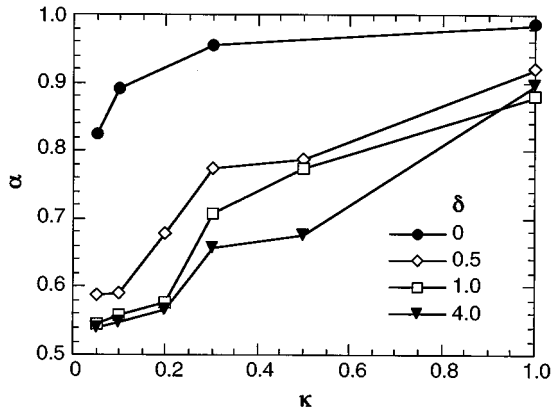

FIG. 14. Surface mass exponent α as a function of sticking coefficient κ and different drift distances δ.

venient and perhaps the most accurate characterization. The objective here is to discuss the trends in the types of site, branch density, density, and average curvature which are apparent in the plots of aggregate growth and are quantified by the geometric quantities. In particular, the open site distribution is a useful quantity with which to characterize the morphology. In the asymptotic growth regime, the distribution of the four neighborhood patterns attains a steady value and is characteristic of the particular simulation parameters employed.

Small drift distances δ and high sticking coefficients κ provide ideal conditions for growing dendrites. The aggregates can be described as nonoverlapping distinct dendritic growths that have well-defined branches, are fractal-like, and have low density. There are a large number of open sites and/or defects in the aggregate growths. The average curvature can be very high and the radii may even be as small as the lattice spacing in extreme cases. At high κ small changes in δ have little effect on morphology. However, the dendrite branches thicken slowly as δ is increased.

At large δ and high κ, the aggregates are dendritic growths that are still fractal-like and have low density. As δ increases further, these grow flatter and more dense. As a result, the aggregate morphology becomes less spiky and more compact. At very large δ the branches of the individual dendrites thicken so much that they overlap. The morphology that results is an amorphous dendrite with high average curvature. There should be some very high δ for all high values of κ at which there is a transition to a dense, compact morphology. These aggregates should be similar to Eden or ballistic clusters [35].

At low δ and low κ, the branches eventually overlap into moderate-density, high-defect, moderate-curvature aggregates except at the lowest δ where some branch structure remains. Even the spikiness of aggregates grown at $\delta=0$ is lower at the smallest κ, and the low-δ aggregates may be solid enough to be considered high-defect compact aggregates. At large δ and low κ, the aggregate growth is a 2D solid with defects that has high average curvature and high density.

The crossover region from dendrite to compact morphologies can be characterized using the results already presented in Sec. IV. The nature of the crossover can be discerned by analyzing the changes in the geometric quantities associated with the open site distribution as the simulation parameters are varied.

At high κ (>0.2) and at all values of δ considered, the aggregate morphology is dendritic. For $\kappa \leqslant 0.2$ a crossover in morphology begins to take place for all δ. The probability of finding sites with large numbers of nearest-neighbor open sites, $P(i=2)$ and $P(i=3)$, decreases and the aggregate growth becomes more compact. The spikiness of the aggregates diminishes and the number of interior occupied sites which are surrounded by four nearest neighbor occupied sites, $P(i=0)$, increases. A high $P(i=0)$ is characteristic of a compact aggregate growth and a low $P(i=0)$ indicates a more dendriticlike, low-density aggregate growth.

The crossover in morphology is demonstrated by the occurrence of peaks in the vacancy density, $P(i=1)$, just below $\kappa=0.2$ for $\delta=0.5$, 1.0, and 4.0. The asymptotic variance of the open site distribution has a high value with a broad peak also near $\kappa=0.2$. Then, at high δ, the variance decreases rapidly as κ is lowered. Peaks in the variance indicate where a particular value of κ occurs for a given δ at which a change in morphology type is starting to take place. The higher the variance, the broader the distribution of the types of sites in the aggregate. There is some onset for a more narrow distribution characterized by a low variance which is more consistent with a solidlike morphology. Near this crossover κ the surface mass exponent α falls rapidly towards 1/2 and ρ increases dramatically. Values of α near 1/2 and ρ near unity characterize a more compact aggregate morphology.

VI. CONCLUSION

The local morphology of the aggregate surface, especially the surface curvature, is determined solely by the drift distance δ and the sticking coefficient κ at a preset source line offset. At any fixed δ, by varying κ, it is possible to obtain a wide range of curvature and density. These two geometric quantities along with others provide extensive morphological information relevant to both modified DLA simulation results and actual electrodeposition experiments. Surface curvature and density in particular have geometric and electrochemical relevance. Their relationship to the simulation parameters δ and κ (which are related to experimental quantities) also reveals the influence of the electrochemical processing conditions on the growth morphology.

Two distinct morphological phases are present in the simulated aggregates grown here: dendritic and compact. Estimates of the values of the simulation parameters at the morphological crossover are obtained from the dependences of mean-square open sites $\langle i^2 \rangle$ on δ and κ. The intrinsic geometric quantities fractal dimension D, density ρ, and $\langle i^2 \rangle$ were found to be useful measures of the openness or compactness of aggregate structure. Crossover values of ρ and D are consistent with the onset of a compact morphology. The aggregate surface curvature is also correlated with ρ, D, and $\langle i^2 \rangle$ through power laws which have δ-dependent parameters.

The crossover radius r^* and the exponent χ do not vary much with drift when $\delta<1$. Aggregate surface curvature is maximal at all κ when $\delta=1$. There is also a bifurcation in the number of available bulk transport directions when δ

$=1$. These and other reasons suggest that $\delta=1$ corresponds to a superpoint at which a change in growth mode or growth mechanism takes place that is accompanied by a change in diffusive behavior. At low δ bulk diffusion is important, but for $\delta \geqslant 1$ bulk transport becomes increasingly ballistic. At large δ the probability that the random walk particle can escape becomes vanishingly small and the particle attaches with a probability of unity. Hence bulk diffusion is insignificant.

Morphological details controlled by local surface kinetics may not always be well described by modified DLA simulations of the type presented here. Any realistic simulation model of electrodeposition must take local surface kinetics into account, especially at low δ (overpotentials). However, morphological pattern formation that is dominated by bulk transport and which only depends on the average or gross features of the electrolyte electrodeposit interface can be well described by the modified DLA simulations and details of morphology and morphological changes are still obtainable over a broad range of simulation parameters.

APPENDIX: MEAN-SQUARE OPEN SITES

The relationship of the mean-square open sites $\langle i^2 \rangle$ to the gradient of the aggregate's density density correlation function $G(r)$ [5,6,39] and average aggregate radius of curvature r is demonstrated here.

In order to find an expression for the mean-square open sites $\langle i^2 \rangle$ in terms of the aggregate's density distribution, consider $i(\mathbf{r}_s)=0, 1, 2, 3$, which is the local representation of the number of open sites adjacent to an occupied site at the position $\mathbf{r}_s$ and is given at any time by

$$i(\mathbf{r}_s)=p(\mathbf{r}_s)\sum_{k=0}^{3} q(\mathbf{r}_k)=p(\mathbf{r}_s)\sum_{k=0}^{3}[1-p(\mathbf{r}_k)]. \quad \text{(A1)}$$

$p(\mathbf{r})$ is the probability that the site at $\mathbf{r}$ is occupied, and $q(\mathbf{r})=1-p(\mathbf{r})$ is the probability that it is unoccupied. In the discrete limit, an occupied site has $p(\mathbf{r}_s)=1$ and an open or unoccupied site has $p(\mathbf{r})=0$. The summation extends to all nearest-neighbor sites $\mathbf{r}_k$ which are adjacent to the occupied site at $\mathbf{r}_s$, but the sites at $\mathbf{r}_k$ may or may not be occupied. Occupied adjacent sites contribute zero to the sum, and open adjacent sites contribute one to the sum. The variable $i(\mathbf{r}_s)$ can be considered a discrete local nearest-neighbor pair correlation between a given occupied site and all adjacent sites.

To evaluate the mean-square open sites $\langle i^2 \rangle$, the expression for $i(\mathbf{r}_s)$ in Eq. (A1) is extended to a continuum where for convenience $\mathbf{r}_s$ is chosen as the origin:

$$i(\mathbf{0})=p(\mathbf{0})\,\frac{1}{a}\int^{\mathbf{a}} d\mathbf{r}\; q(\mathbf{r}')=p(\mathbf{0})q(\mathbf{a})$$
$$=p(\mathbf{0})\left(q(\mathbf{0})+a\nabla q(\mathbf{a})\cdot\frac{\mathbf{a}}{a}\right)+O(a^2). \quad \text{(A2)}$$

Here a is the lattice spacing which is assumed to be a small parameter and $O(\epsilon)$ means on the order of ϵ. A Taylor series expansion has been made. Next, square this expression for $i(\mathbf{0})$ and average over the probability density $P(\mathbf{r}_s, i(\mathbf{r}_s))$, replacing $q(\mathbf{r})$ by $1-p(\mathbf{r})$. Averages are denoted by brackets:

$$\langle i(\mathbf{0})^2\rangle=\langle p(\mathbf{0})^2[1-p(\mathbf{0})]^2\rangle$$
$$+2a\langle p(\mathbf{0})^2[1-p(\mathbf{0})]\nabla[1-p(\mathbf{a})]\rangle\cdot\frac{\mathbf{a}}{a}+O(a^2). \quad \text{(A3)}$$

It can be assumed that $\langle p(0)^n\rangle=1$, $n>0$, and so the first term vanishes. The average $O(a)$ can be simplified if a Gaussian distribution is assumed for the occupation probabilities. The average of the gradient of $p(\mathbf{a})$ alone is assumed to vanish. Radial symmetry is next assumed, and in that case the gradient of $p(\mathbf{a})$ is in the direction of $\mathbf{a}$. The gradient is symmetrized.

The occupation probability $p(\mathbf{r})$ and the local density operator $n(\mathbf{r})$ are related in a coarse sense by $p(\mathbf{r})=n(\mathbf{r})/n_0$, where n_0 is a normalization factor. The density density correlation function is $G(\mathbf{r}-\mathbf{r}')=\langle n(\mathbf{r})n(\mathbf{r}')\rangle$ [5,6,39]. It follows that

$$\langle i^2\rangle=a|\nabla\langle p(\mathbf{0})p(\mathbf{a})\rangle|=a\left|\frac{\nabla G(a)}{n_0^2}\right|+O(a^2). \quad \text{(A4)}$$

The mean-square open sites are related to the magnitude of the gradient of $G(r)$ when evaluated at a distance equal to the nearest-neighbor lattice spacing. Through their relation to $G(r)$, the geometric quantities $\langle i^2\rangle$ and D, and ρ also, are measures of the openness or compactness of an aggregate growth and can be used to quantify aggregate morphology. In particular, $\langle i^2\rangle$ is a very robust statistic because it is an exponent and is insensitive to small changes in the spatial distribution of particles in aggregate.

It is shown here that the average surface curvature $\langle K\rangle = 1/r$ of the aggregates grown in the modified DLA simulations is related to $\langle i^2\rangle$ by a power law. $\langle K\rangle$ can be calculated approximately using a statistical mechanical approach [40]. The unit mean normal $\mathbf{N}(\mathbf{r})$ to the aggregate surface is curl free and can be expressed as the negative of the gradient of a mean potential. The mean local curvature is the divergence of $\mathbf{N}(\mathbf{r})$ and is the source for the mean potential in Poisson's equation. $\mathbf{N}(\mathbf{r})$ is in the direction of the gradient of the local density. Through a normalization condition it can be shown that $\langle K\rangle$ is approximately

$$\langle K\rangle=\int_s d\sigma\;\mathbf{N}\cdot P_1(\mathbf{r})\,\frac{\nabla P_1(\mathbf{r})}{\nabla P_1(\mathbf{r})\cdot\mathbf{N}}, \quad \text{(A5)}$$

where $P_1(\mathbf{r})$ is the one-particle aggregate position distribution function (effectively the local density).

The mean-square open sites are

$$\langle i^2\rangle=V^2a|\nabla P_2(\mathbf{a},0)|$$
$$=V^2aP_1(\mathbf{0})|\nabla\{P_1(\mathbf{a})[1+M_2(\mathbf{a},\mathbf{0})]\}|. \quad \text{(A6)}$$

In Eq. (A6), $G(\mathbf{r},\mathbf{r}')=V^2P_2(\mathbf{r},\mathbf{r}')$, where $P_2(\mathbf{r},\mathbf{r}')$ is the two-particle aggregate position distribution function and $M_2(\mathbf{r},\mathbf{0})$ is the pair correlation function [41]. Since, in a first approximation, the mean potential and hence the mean local

curvature do not see the correlations [40], let $M_2(\mathbf{r},\mathbf{0})=0$ in this expression. The mean-square open sites are then

$$\langle i^2\rangle = V^2 a|P_1(0)\nabla P_1(\mathbf{a})| = V^2 a P_1(0)\mathbf{N}\cdot\nabla P_1(\mathbf{a}). \tag{A7}$$

If in Eq. (A5) the surface is taken at the lattice spacing a and the arguments are assumed to be constant, it follows that

$$\langle K\rangle = \Delta A P_1(\mathbf{a})\mathbf{N}\cdot\frac{\nabla P_1(\mathbf{a})}{\nabla P_1(\mathbf{a})\cdot\mathbf{N}}, \tag{A8}$$

where ΔA is the area of the surface at the point a. Now $\langle i^2\rangle = Ca\langle K\rangle$, where

$$C = \frac{V^2 P_1(\mathbf{0})}{\Delta A}\,\frac{\nabla P_1(\mathbf{a})\cdot\mathbf{N}}{P_1(\mathbf{a})}. \tag{A9}$$

The expression for the constant C is simply a Gibbs-Thompson condition [40] and is of order unity.

[1] J. Bockris and G. Razumney, *Fundamental Aspects of Electrocrystalization* (Plenum, New York, 1967).
[2] J. Barton and J. Bockris, Proc. R. Soc. London, Ser. A **268**, 485 (1962).
[3] A. Despic, in *Comprehensive Treatise of Electrochemistry*, edited by B. Conway (Plenum, New York, 1983), Vol. 7.
[4] J. Bockris and A. Damjanovic, *Modern Aspects of Electrochemistry 3* (Butterworths, London, 1964).
[5] T. Witten and L. Sander, Phys. Rev. Lett. **47**, 1400 (1981).
[6] T. Witten and L. Sander, Phys. Rev. B **27**, 5686 (1983).
[7] M. Matsushita, M. Sano, Y. Hayakawa, H. Honjo, and Y. Sawada, Phys. Rev. Lett. **53**, 286 (1984).
[8] Y. Sawada, A. Doughtery, and J. Gollub, Phys. Rev. Lett. **56**, 1260 (1986).
[9] D. Grier, E. Ben-Jacob, R. Clarke, and L. Sander, Phys. Rev. Lett. **56**, 1265 (1986).
[10] E. Ben-Jacob, G. Deutscher, P. Garik, N. Goldenfield, and Y. Lareah, Phys. Rev. Lett. **57**, 903 (1986).
[11] F. Argoul, A. Arnado, and G. Grasseau, Phys. Rev. Lett. **61**, 2558 (1988).
[12] R. Sutor and P.-Z. Wong, Phys. Rev. B **39**, 4536 (1989).
[13] P. Meakin, Phys. Rev. B **28**, 5221 (1983).
[14] R. Jullien, M. Kolb, and R. Botet, J. Phys. (France) **45**, 395 (1984).
[15] R. Kapral, S. Whittington, and R. Desai, Phys. Rev. A **19**, 1727 (1986).
[16] R.-F. Xiao, J. Alexander, and F. Rosenberger, Phys. Rev. A **39**, 6397 (1989).
[17] R.-F. Xiao, J. Alexander, and F. Rosenberger, Phys. Rev. A **38**, 2447 (1988).
[18] R.-F. Xiao, J. Alexander, and F. Rosenberger, J. Cryst. Growth **100**, 313 (1990).
[19] R.-F. Xiao, J. Alexander, and F. Rosenberger, Phys. Rev. A **43**, 2977 (1991).
[20] R. Smith and S. Collins, Phys. Rev. A **39**, 5409 (1989).
[21] M. Kac, in *Selected Papers on Noise and Stochastic Processes*, edited by N. Wax (Dover, New York, 1959).
[22] W. Feller, *An Introduction to Probability Theory and its Applications* (Wiley, New York, 1968), Vols. 1 and 2.
[23] W. Feller, Ann. Math. **55**, 468 (1952).
[24] J. Bockris and R. Reddy, *Modern Electrochemistry* (Plenum, New York, 1970), Vols. 1 and 2.
[25] F. Rosenberger, *Fundamentals of Crystal Growth* (Springer-Verlag, Berlin, 1979).
[26] S. Eskinnazi, *Principles of Fluid Mechanics*, 2nd ed. (Allyn and Bacon, Boston, 1968).
[27] W. Moore, *Physical Chemistry*, 4th ed. (Prentice-Hall, Englewood Cliffs, NJ, 1972).
[28] J. Goodisman, *Electrochemistry: Theoretical Foundations* (Wiley, New York, 1987).
[29] A. Adamson, *Physical Chemistry of Surfaces*, 5th ed. (Wiley, New York, 1990).
[30] J. Davies, and E. Rideal, *Interfacial Phenomena* (Academic, New York, 1963).
[31] R. Tolman, J. Chem. Phys. **17**, 333 (1949).
[32] J. Melrose, Ind. Eng. Chem. Res. **60**, 53 (1968).
[33] R. Voss, Phys. Rev. B **30**, 334 (1984).
[34] R. Voss and J. Tomkiewicz, J. Electrochem. Soc. **132**, 371 (1985).
[35] H. Stanley and N. Ostrowsky, in *On Growth and Form: Fractral and Non-Fractal Patterns in Physics*, NATO Advanced Study Institute, Series B: Physics (Nijhoff, Dordrecht, 1985).
[36] R. L. Burden and J. D. Faires, *Numerical Analysis*, 4th ed. (PWS/Kent, Boston, 1989).
[37] R. Ellis and D. Gulick, *Calculus with Analytical Geometry*, 3rd ed. (Harcort Brace Jovanovich, New York, 1986).
[38] Y. Saito and T. Ueta, Phys. Rev. A **40**, 3408 (1989).
[39] H. Stanley, *Introduction to Phase Transitions and Critical Phenomena* (Oxford University Press, Oxford, 1971).
[40] S. Hill and J. I. D. Alexander (unpublished).
[41] R. Balescu, *Equilibrium and Nonequilibrium Statistical Mechanics* (Wiley, New York, 1975).